

面向稀疏波分复用系统的超大带宽硅基光子滤波器

廖莎莎^{1,2*}, 黄琮¹, 冯玉婷¹, 张伍浩¹, 赵帅¹, 刘真伟¹¹重庆邮电大学通信与信息工程学院, 重庆 400065;²上海交通大学区域光纤通信网与新型光通信系统国家重点实验室, 上海 200240

摘要 大带宽光子滤波器被广泛应用于稀疏波分复用系统中,而在硅基芯片上实现结构紧凑、性能优良的超大带宽滤波器仍然是该领域研究的重点。提出一种基于光栅辅助反向耦合器的超大带宽硅基光子滤波器。利用窄波导更低有效折射率和更分散电场分布的性质,实现了带宽为 92.9 nm、器件长度为 250.6 μm 的超大带宽滤波器。该滤波器具有矩形度高、带宽大、损耗低等优势,能满足稀疏波分复用系统中解复用等需求。

关键词 集成光学; 稀疏波分复用; 硅光子学; 滤波器; 光子集成电路

中图分类号 TN256

文献标志码 A

DOI: 10.3788/AOS221523

1 引言

随着科技信息技术的不断发展,人们对通信系统容量和速度的需求日益增加,其中波分复用技术在提升系统容量方面发挥着重要的作用。在城域网等应用中,由于通道数量远小于骨干网,对激光器的要求也较低,通常采用信道间隔可达 20 nm 的稀疏波分复用(CWDM)系统^[1-2]。解复用器作为 CWDM 系统的关键组成部分,成为该领域的研究热点。目前,主要利用高矩形度的大带宽滤波器来实现解复用的功能。近年来,大带宽和超大带宽的滤波器方案被频繁提出和实现,采用的器件结构包括光子晶体^[3-6]、马赫-曾德尔干涉仪(MZI)^[7-8]、波导布拉格光栅^[9-11]等。Sah 等^[12]在脊波导上设计了一种非对称多模波导光栅结构,实现了带宽约为 40 nm 的带通滤波器。Huang 等^[13]提出了一种基于多模一维光子晶体方案,该方案将两个多模光子晶体波导级联,最终实现带宽最大可达 84 nm、旁瓣抑制比大于 20 dB、长度仅为 40 μm 的超紧凑滤波器。Sumi 等^[14]提出切趾型亚波长光栅波导方案,实现了最大带宽达到 100 nm、旁瓣抑制比大于 30 dB、插入损耗为 0.5 dB 的超大带宽滤波器。以上这些结构虽然具有良好的滤波特性,但由于它们工作在反射模式,后续分离反射信号时需添加额外的光环形器等磁光器件,这无疑增加了系统的复杂度;而且磁光材料难以与硅

基器件大规模集成,也影响了上述方案的应用范围。采用光栅辅助的反向耦合器可以通过介电扰动将特定的波长信号下载到另一波导中,实现反向传输信号的分离,所以成为大带宽滤波器的重点研究结构。Charron 等^[15]提出将亚波长光栅(SWG)与非对称波导光栅相结合,实现了带宽为 33.4 nm、旁瓣抑制比为 3 dB 的滤波器。为了提高频谱利用率,Boroojerdi 等^[16]提出了级联光栅辅助反向耦合器方案,通过热调的方式,最终实现了带宽调节范围为 1.1~11.7 nm 的滤波器。为了进一步增加带宽,Yun 等^[17]将高斯切趾函数运用在 SWG 辅助反向耦合器中,实现了 3 dB 带宽为 32.6 nm、旁瓣抑制比为 19 dB、插入损耗为 0.26 dB 的宽带滤波器。Hammond 等^[18]利用周期啁啾技术,实现了带宽高达 88.1 nm 的光栅辅助反向耦合器,但是器件总长度为 4.7 mm,难以大规模集成。综上所述,传统的光栅辅助和 SWG 辅助反向耦合器方案可实现的带宽有限,绝大部分带宽 <40 nm。超大带宽(>80 nm)滤波器的尺寸较大,难以满足大规模集成的需求^[18]。因此,在保证超大带宽的基础上,缩小器件尺寸是目前 CWDM 解复用器的研究关键。

为了实现紧凑的超大带宽滤波器,本文提出一种基于光栅辅助反向耦合器结构的滤波器方案,该方案利用窄波导具有更低有效折射率和更分散电场的性质,通过将输入波导经过 Taper 逐渐变为窄波导,实现

收稿日期: 2022-07-25; 修回日期: 2022-09-13; 录用日期: 2022-10-14

基金项目: 重庆市自然科学基金面上项目(cstc2019jcyj-msxmX0597)、上海交通大学区域光纤通信网与新型光通信系统国家重点实验室开放基金(2021GZKF005)

通信作者: *liaoss@cqupt.edu.cn

超大带宽滤波器。通过合理地设计结构参数,最终可实现带宽为92.9 nm、形状因子(3 dB带宽与10 dB带宽之比)为0.99、器件长度为250.6 μm的超大带宽硅基光子滤波器。除此之外,本文还分析了工艺误差对该滤波器方案性能的影响,并提供了相应的解决方案。该滤波器具有超大宽带、高矩形度、低损耗等优势,能广泛应用于CWDM通信系统中。

2 超大带宽滤波器的理论推导

传统光栅辅助反向耦合器方案的结构示意图如图1(a)所示,该结构通常由两根不同宽度的波导光栅组成,当两者的传播常数相差较大时,同向耦合效率很低,甚至截止。光栅梳齿对折射率的调制,使得满足相位匹配条件的输入光信号反向耦合进入下方波导,并从下载(drop)端输出,而不满足该条件的光信号则从直通(through)端输出。根据前期的工作^[19],drop端输出信号的带宽主要受波导有效折射率和耦合系数的影响,其表达式为

$$B_{3dB} = \frac{2\lambda_0^2}{\pi(n_1 + n_2)} |\kappa|, \quad (1)$$

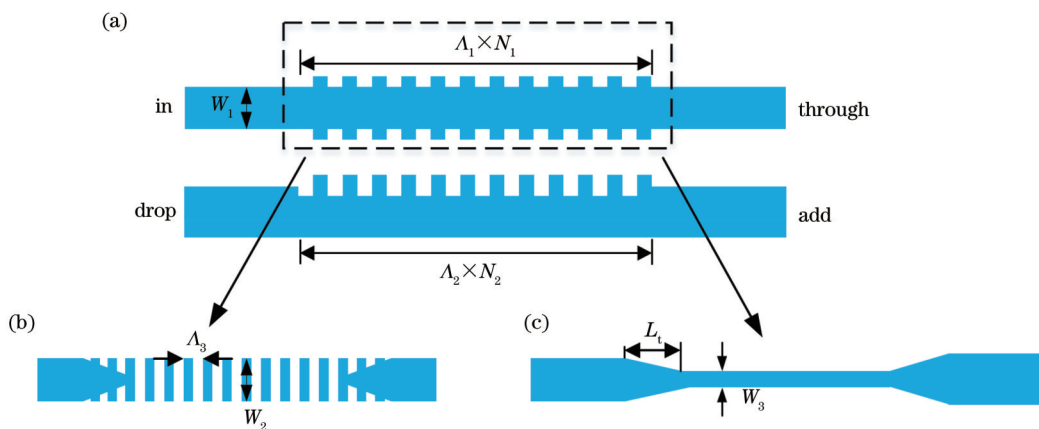


图1 光栅辅助反向耦合器方案结构示意图。(a)传统光栅;(b)SWG;(c)窄波导

Fig. 1 Schematic of grating assisted contra-directional couplers. (a) Traditional grating; (b) SWG; (c) narrow waveguide

为了克服上述缺点,将图1(a)的虚线框部分更改为窄波导结构,如图1(c)所示。通过将常规单模波导拉锥至窄波导,可以进一步减小 n_1 和 n_2 、增大模式重叠积分。图2(a)、(b)展示了不同结构下波导的有效折射率和电场强度分布的变化情况。为了方便比较,传统光栅和SWG的宽度 W_1 和 W_2 均选择500 nm,占空比均为0.5,传统光栅的周期 Λ_1 为310 nm;SWG的周期 Λ_3 为206 nm。窄波导宽度 W_3 为180 nm,Taper的长度 L_t 为8 μm。

由图2(a)可知,窄波导在1530~1570 nm波长范围内的有效折射率为1.441~1.447,而传统光栅和SWG在相同波长范围内有效折射率分别为2.421~2.467和1.693~1.718,即窄波导的有效折射率小于传统光栅和SWG的有效折射率。在1550 nm波长下,

式中: λ_0 为反向耦合中心波长; n_1 和 n_2 分别表示上方和下方波导的有效折射率; κ 为耦合系数。

$$\kappa = \frac{\omega}{4} \int E_1^*(x, y) \times \epsilon(x, y) \times E_2(x, y) dx dy, \quad (2)$$

式中: $E_1(x, y)$ 和 $E_2(x, y)$ 分别为两个波导中模式的归一化电场分布; $\epsilon(x, y)$ 为周期性介电扰动的一阶傅里叶展开系数; ω 为光的角频率。从式(1)可以看出,反向耦合器的带宽反比于两波导有效折射率之和(n_1+n_2),正比于耦合系数 κ 。因此,为提升滤波器的带宽,需减小 n_1 、 n_2 ,并增大 κ 。由式(2)可知,在 $\epsilon(x, y)$ 不变的情况下,两个光场的模式重叠积分将直接影响 κ 的大小,因此可以通过改变波导结构来增加模式积分。在前期的工作^[19]中将图1(a)的虚线框部分改为SWG结构[图1(b)],SWG的加入可以有效减小 n_1 、 n_2 ,并增大模式重叠积分(其有效折射率和电场强度分布情况如图2所示),最终实现了带宽为64.07 nm的滤波器。该方案对制备工艺要求较高,其中SWG的梳齿宽度为560 nm,梳齿长度仅103 nm;施加切趾函数后,梳齿在纵向位置上的最大偏置仅为48 nm,工艺复杂度较高、容差较小。

窄波导、传统光栅和SWG沿波导宽度方向(y)的电场分布图如图2(b)所示,其中实线和短虚线分别为窄波导和传统光栅中心处电场强度的分布曲线,长虚线和星型线分别为SWG中Si与SiO₂区域电场强度的分布曲线。可以明显看出,窄波导结构电场强度在波导外侧分布更多,因此在微扰幅度及耦合间隙相同的情况下,窄波导通过式(2)计算得到的耦合系数会更大,从而使滤波器具有更大的带宽。

为了利用该滤波器实现较大的带宽,可以采用文献[20]中的将耦合区域划分为多段的方式,采用传输矩阵法来计算其光谱特性。假设光栅周期 Λ_2 为390 nm, κ 为0.18 μm⁻¹,两个波导的有效折射率分别为 $n_1=1.47$ 、 $n_2=2.5$ 。光栅个数 $N_2=600$,并每隔一个光栅周期分为一段。最终计算得到大带宽滤波器的传

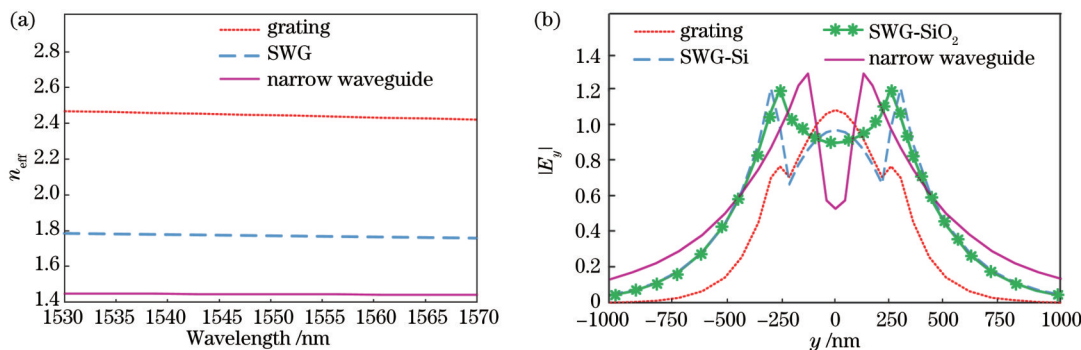


图 2 不同波导参数对比。(a)有效折射率随波长的变化关系;(b)电场强度随波导宽度分布

Fig. 2 Parameter comparison of different waveguide structures. (a) Effective refractive index varies with the wavelength; (b) electric field intensity distribution varies with the width of the waveguide

输特性如图 3 所示。

图 3 中实线表示 through 端的输出谱,虚线表示 drop 端的输出谱。此时,drop 端 3 dB 带宽为 70 nm,大于文献[19]中实现的带宽,符合上述理论推导。图 3 中插图显示的是通带左边缘的旁瓣,从插图可以看出,

滤波器的旁瓣抑制比仅有 0.15 dB。因此,窄波导虽然能有效增加滤波器带宽,但得到的滤波器旁瓣抑制比较低,会导致相邻通道间具有较高的串扰。因此,本文将进一步利用切趾技术来提升滤波器的旁瓣抑制比。

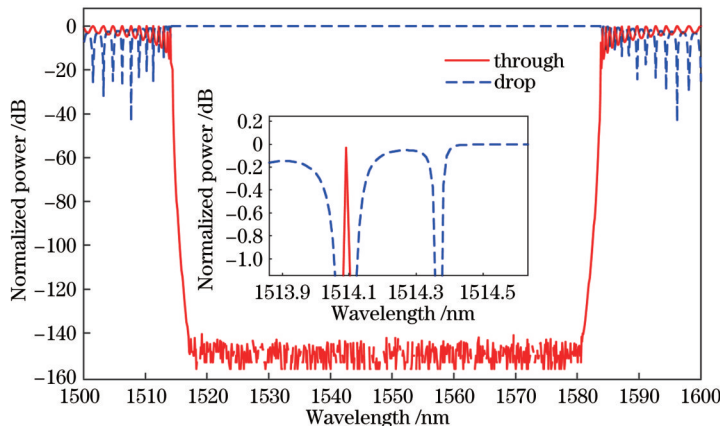


图 3 基于窄波导的大带宽滤波器 through 端口和 drop 端口的输出谱线

Fig. 3 Output spectra of the through and drop ports of broad bandwidth filter based on the narrow waveguide

3 超大带宽滤波器的设计与优化

滤波器的旁瓣较高主要是耦合系数的突变不连续引起的。为了解决该问题,可以利用切趾技术来实现耦合系数的缓慢变化。最常见的光栅切趾为梳齿切趾,如图 4 左上图所示。然而仅对梳齿切趾往往会造成单旁瓣效应^[21],无法同时压低两侧旁瓣。因此可以结合波导切趾的结构,如图 4 右上图所示。根据前期成果^[20],同时对光栅梳齿和波导进行切趾,不但可以降低两侧旁瓣,还可以减小因切趾引起的反向耦合波长偏移,其结构示意图如图 4 下图所示。

切趾后滤波器的结构示意图如图 5 所示。采用的 SOI 材料具有 220 nm 的顶层硅和 3 μm 的掩埋层,其中下侧波导中弯曲波导前后各加入了一段直波导,长度 \$L_e=1.5 \mu\text{m}\$, drop 端波导宽度 \$W_4=420 \text{ nm}\$, 圆弧的半径 \$R=8 \mu\text{m}\$。光栅的周期 \$\Lambda_4=386 \text{ nm}\$, 个数 \$N_3=600\$,

波导间距 \$G=180 \text{ nm}\$。

下方波导的光栅耦合区被施加高斯切趾函数: \$W_{g1,2} \times \exp \{-2[\alpha_{1,2}(i-0.5N)/N]^2\}\$, 其中 \$W_{g1}, W_{g2}\$ 分别为光栅齿最大宽度及波导最深凹陷深度, \$\alpha_1, \alpha_2\$ 为对应的高斯系数, \$N\$ 为光栅的周期数。经过 2.5D varFDTD 算法多次优化后,发现当 \$W_{g1}=96.5 \text{ nm}\$, \$W_{g2}=100 \text{ nm}\$、\$\alpha_1=1.83\$、\$\alpha_2=1.75\$ 时,滤波器的旁瓣抑制效果最好,其结构参数如表 1 所示,传输谱如图 6 所示,实线和虚线分别代表切趾前后 drop 端的输出谱线。可以看出,切趾后旁瓣抑制比明显增大。此时,滤波器 3 dB 带宽为 92.9 nm,旁瓣抑制比大于 11.1 dB,形状因子为 0.99,插入损耗小于 0.38 dB,带内纹波(通带内最大功率与最小功率之比)小于 0.28 dB。

通过降低耦合系数的方法,可以进一步提高旁瓣抑制比,然而这会导致带宽减小。在综合权衡滤波器带宽和旁瓣抑制比的基础上,本文设计了一种紧凑的

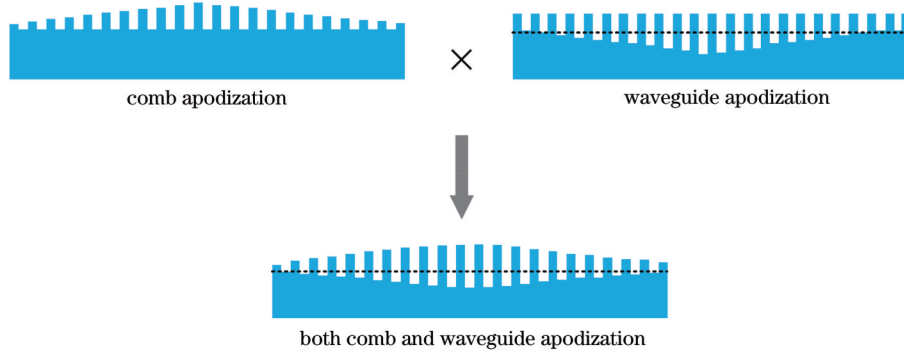


图4 不同切趾结构示意图
Fig. 4 Schematic of different apodization

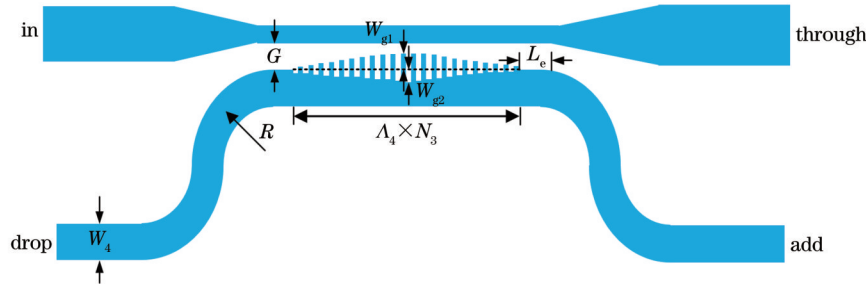


图5 切趾后的大带宽滤波器结构示意图
Fig. 5 Schematic of broad bandwidth filter after apodization

表1 超大带宽滤波器的结构参数

Table 1 Structural parameters of ultra-wide bandwidth filter

Parameter	W_3 /nm	W_4 /nm	W_{g1} /nm	W_{g2} /nm	α_1	α_2	A_4 /nm	N_3	G /nm
Value	180	420	96.5	100	1.83	1.75	386	600	180

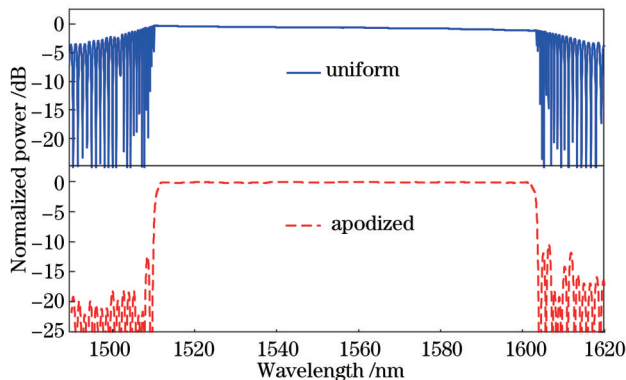


图6 切趾与均匀的超大带宽滤波器传输谱
Fig. 6 Transmission spectra of the apodized and the uniform ultra-wide bandwidth filter

高旁瓣抑制比、大带宽滤波器。在其他参数不变的情况下,使 $W_3=181$ nm、 $W_4=422$ nm、 $A_4=385$ nm、 $N_3=200$ 、 $G=200$ nm、 $W_{g1}=97$ nm、 $\alpha_1=3.1$ 、 $\alpha_2=2.5$,可以

达到良好的旁瓣抑制效果,其结构参数如表2所示,传输谱如图7所示。

图7中实线表示通过端的输出谱线,虚线表示

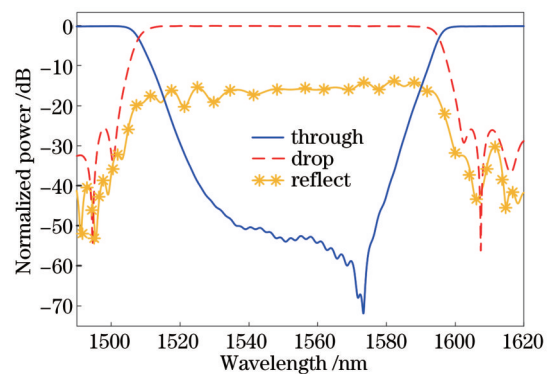


图7 紧凑的高旁瓣抑制比、大带宽滤波器传输谱
Fig. 7 Transmission spectra of the compact, high sidelobe rejection ratio, and broad bandwidth filter

表2 紧凑的高旁瓣抑制比、大带宽滤波器的结构参数

Table 2 Structural parameters of the compact, high sidelobe rejection ratio, and broad bandwidth filter

Parameter	W_3 /nm	W_4 /nm	W_{g1} /nm	W_{g2} /nm	α_1	α_2	A_4 /nm	N_3	G /nm
Value	181	422	97	100	3.1	2.5	385	200	200

drop的输出谱线,星型线表示反射(reflect)端的输出谱。此时drop端3 dB带宽为87 nm,旁瓣抑制比为25.6 dB,形状因子为0.94,插入损耗小于0.16 dB,带内纹波小于0.08 dB。相比所设计的方案1,在滤波器带宽只减小6%的情况下,旁瓣抑制比提高了129%。此外,该结构的长度仅为96 μm ,相比之前的设计減少了61.7%,更加适用于对旁瓣抑制比、尺寸要求较高的应用场景。

表3 不同大带宽滤波器方案的性能比较
Table 3 Comparison of the performances of different broad bandwidth filter schemes

Ref.	3 dB bandwidth /nm	Length / μm	Sidelobe suppression ration /dB	Insertion loss /dB	Contra-directional coupling type or not
[12]	40	~100	25	/	No
[13]	84	~40	20	0.04	No
[14]	100	~70	30	0.5	No
[15]	33.4	~150	3	/	Yes
[16]	11.7	~730	31	2.6	Yes
[17]	32.6	~422	19	0.26	Yes
[18]	88.1	~4700	9.7	1.77	Yes
[19]	64.07	~400	10.5	0.6	Yes
Scheme 1	92.9	~250.6	11.1	0.38	Yes
Scheme 2	87	~96	25.6	0.16	Yes

器件在制造过程中难免存在工艺误差,导致尺寸偏离设计值。一般情况下,结构尺寸越小,工艺误差对性能的影响越大。因此,本文着重分析了紧凑型滤波器中光栅切趾系数和光栅梳齿宽度的误差对滤波器性能的影响。当高斯切趾系数 α_1, α_2 存在 ± 0.5 的偏差时,与原参数相比,光栅最小特征尺寸变化了 $0\sim 11$ nm,此时的滤波器性能如图8(a)所示。经计算可以得出,3 dB带宽均大于86.9 nm,形状因子大于0.92,插入损耗均小于0.29 dB,带内纹波小于0.15 dB,性能变化并不明显。只有旁瓣抑制比劣化较为严重,当 $\alpha_1=2.6, \alpha_2=3$ 时,旁瓣抑制比最小,为10.7 dB。但对于一般滤波场景,该旁瓣抑制比仍能满足

所提出的两种超大带宽滤波器方案与以往的宽带滤波器性能比较如表3所示。由表3可知,所提出的两种方案在带宽上具有较大优势,其中:方案1实现了92.9 nm的3 dB带宽,相比于同样采用反向耦合方式的文献[18]带宽增加了5%,尺寸缩小约95%;方案2在保持大带宽的基础上,进一步提高了旁瓣抑制比、缩小了器件的长度。与采用反向耦合方式的文献[15-19]相比,所提方案在带宽、尺寸方面均有着明显的优势。

足滤波需求。对于旁瓣抑制比要求较高的应用场景,可以通过采用适当增加窄波导与光栅间的间隔G设计值的方法,抵消工艺误差的影响。当 $\alpha_1=2.6, \alpha_2=3$ 时,增大G后,滤波器输出谱如图8(b)所示。经计算可以发现:当G=210 nm时,旁瓣抑制比可以提高到26.9 dB;当G=230 nm时,旁瓣抑制比为14 dB,依然优于之前的10.7 dB。因此,可在制备滤波器时就将G值适当增大,这样即使存在工艺误差,也能有效保证旁瓣抑制比。该方法会损失一部分滤波器带宽,比如:当G=210 nm时,带宽减小了1.4 nm;当G=230 nm时,带宽减小了5.7 nm。所以,在实际制备过程中,应根据实际应用场景需求,优化相关结构参数。

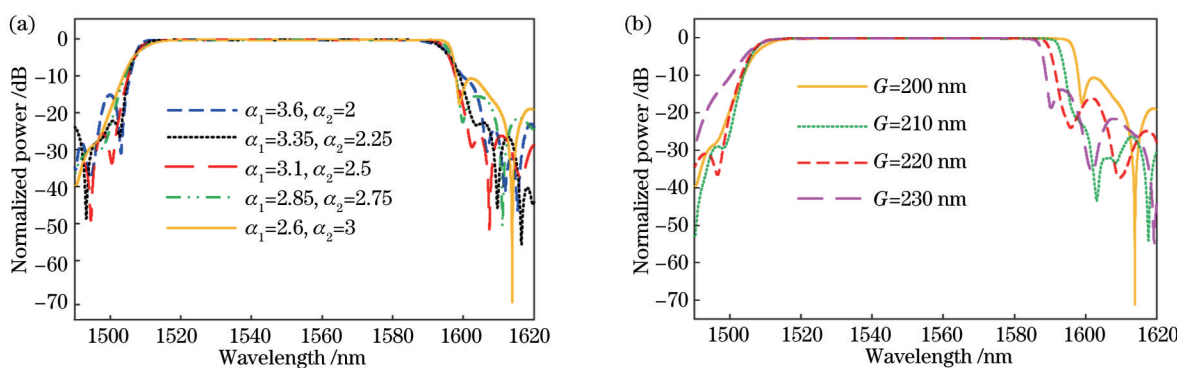


图8 高斯系数 α_1, α_2 和G存在偏差时,滤波器的滤波谱线。(a)不同 α_1, α_2 下drop端的输出谱;(b)调控G时drop端的输出谱
Fig. 8 Spectra of the filter varied with Gaussian coefficients α_1, α_2 , and G . (a) Spectra on drop port under different Gaussian coefficients α_1 and α_2 ; (b) spectra on drop port by controlling G

当光栅齿宽 W_{g1} 与光栅凹陷深度 W_{g2} 同时存在 $\pm 15 \text{ nm}$ 的偏差时,本文挑选了滤波谱线变化较为明显的情况,并绘制在图9中。经计算可知,滤波器旁瓣抑制比均大于 17 dB , 3 dB 带宽均大于 83.4 nm ,形状因子均大于 0.93 ,插入损耗小于 0.22 dB ,带内纹波小于 0.1 dB 。因此,工艺误差对滤波器矩形度等方面的影响较小,但滤波器的中心波长会出现明显的漂

(约 20 nm),这是由光栅结构有效折射率增大导致的。为了降低工艺误差对中心波长的影响,可以在制备时微调光栅周期,通过制备多组不同周期的滤波器,将中心波长调整至所需的工作波段。滤波器中其他结构参数,如波导长度和宽度等,因本身尺寸较大,工艺误差对其影响较小,故不再做专门讨论。

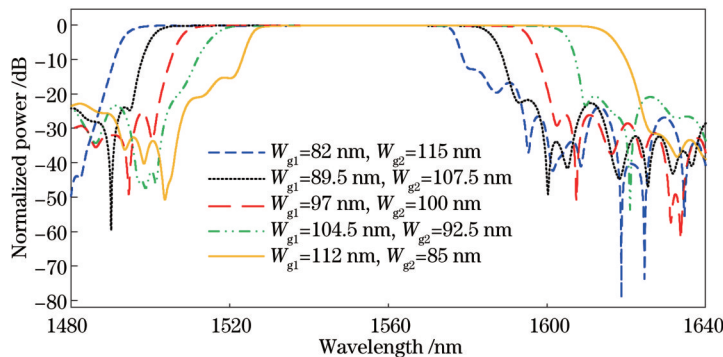


图9 光栅参数 W_{g1} 、 W_{g2} 存在偏差时,drop端的输出谱线
Fig. 9 Output spectra of the drop port varied with W_{g1} and W_{g2}

4 结 论

提出一种基于光栅辅助反向耦合器的超大带宽滤波器。首先,根据耦合模理论,推导了滤波器带宽的表达式,分析了带宽的影响因素;其次,结合前期的工作,提出了将反向耦合器中的一根波导更改为窄波导的方法;最后,对该结构进行了设计和优化,最终实现了 3 dB 带宽为 92.9 nm ,旁瓣抑制比为 11.1 dB ,形状因子为 0.99 ,插入损耗为 0.38 dB ,带内纹波为 0.28 dB 的超大带宽硅基光子滤波器。除此之外,本文还设计了一种结构更加紧凑、旁瓣抑制比更高的滤波器方案,通过再次优化,实现了 3 dB 带宽为 87 nm ,旁瓣抑制比为 25.6 dB ,器件长度为 $96 \mu\text{m}$,插入损耗为 0.16 dB ,带内纹波为 0.08 dB 的滤波器。所提出的两种滤波器方案均采用反向耦合方式,相比于文献[15-16]的同类型滤波器在带宽和尺寸上均有明显优势。方案1中滤波器带宽大于同类结构的带宽最大的已有方案(文献[18]),并大大缩小了滤波器尺寸。方案2进一步提高了旁瓣抑制比、缩小了器件的长度,适用于对旁瓣抑制比、尺寸更为敏感的应用场景。此外,本文还重点分析了滤波器中光栅切趾系数和光栅梳齿宽度存在工艺误差时滤波器性能的变化,并提出了增加窄波导与光栅间的间隔 G 设计值和微调光栅周期的方法降低工艺误差对滤波器性能的影响。所提出的超大带宽滤波器方案具有矩形度高、尺寸小、损耗低等优势,能广泛应用于CWDM系统中。

参 考 文 献

- [1] 李梦凡,陈德媛,张岩,等.可扩展小型化光子晶体波分复用

- 器研究[J].激光与光电子学进展,2021,58(23):2325001.
Li M F, Chen D Y, Zhang Y, et al. Research on scalable and miniaturized photonic crystal wavelength division multiplexer[J]. Laser & Optoelectronics Progress, 2021, 58(23): 2325001.
[2] 曹东东,王明月,李将,等.光纤保密通信中的全光同步方案设计与实现[J/OL].中国激光:1-18[2022-06-14].<http://kns.cnki.net/kcms/detail/31.1339.tn.20220713.1937.342.html>.
Cao D D, Wang M M, Li J, et al. Design and implementation of all-optical synchronization scheme in optical fiber secure communication[J/OL]. Chinese Journal of Lasers:1-18[2022-06-14].<http://kns.cnki.net/kcms/detail/31.1339.tn.20220713.1937.342.html>.
[3] 徐聪,陈德媛,李宜书,等.无磁性光子晶体类T型非互易性双通道滤波器设计[J].激光与光电子学进展,2022,60(5):0523003.
Xu C, Chen D Y, Li Y S, et al. Design of T-type nonreciprocal two channel filter based on non-magnetic photonic crystal[J]. Laser & Optoelectronics Progress, 2022, 60(5): 0523003.
[4] Khonina S N, Kazanskiy N L, Butt M A. Spectral characteristics of broad band-rejection filter based on Bragg grating, one-dimensional photonic crystal, and subwavelength grating waveguide[J]. Physica Scripta, 2021, 96(5): 055505.
[5] Prakash C, Sen M, Mondal H, et al. Design and optimization of a TE-pass polarization filter based on a slotted photonic crystal waveguide[J]. Journal of the Optical Society of America B, 2018, 35(8): 1791-1798.
[6] Koshiba M. Wavelength division multiplexing and demultiplexing with photonic crystal waveguide couplers[J]. Journal of Lightwave Technology, 2001, 19(12): 1970-1975.
[7] Yang H M, Li J, Zheng P F, et al. A stopband and passband switchable microwave photonic filter based on integrated dual ring coupled Mach-Zehnder interferometer[J]. IEEE Photonics Journal, 2019, 11(4): 5502608.
[8] Wang M, Chen X F, Khan U, et al. Programmable wavelength filter with double ring loaded MZI[J]. Scientific Reports, 2022, 12: 1482.
[9] Butt M A, Khonina S N, Kazanskiy N L. A compact design of a modified Bragg grating filter based on a metal-insulator-metal waveguide for filtering and temperature sensing applications[J].

- Optik, 2022, 251: 168466.
- [10] Pereira-Martin D, Luque-González J M, Wangüemert-Pérez J G, et al. Complex spectral filters in silicon waveguides based on cladding-modulated Bragg gratings[J]. Optics Express, 2021, 29 (11): 15867-15881.
- [11] Jiang J F, Qiu H Y, Wang G C, et al. Broadband tunable filter based on the loop of multimode Bragg grating[J]. Optics Express, 2018, 26(1): 559-566.
- [12] Sah P, Das B K. Broadband wavelength filter device using a sidewall grating in multimode SOI rib waveguide[C]/Optical Fiber Communication Conference, March 19-23, 2017, Los Angeles, California. Washington, D. C.: Optica Publishing Group, 2017: Th1G.1.
- [13] Huang Q Z, Jie K, Liu Q, et al. Ultra-compact, broadband tunable optical bandstop filters based on a multimode one-dimensional photonic crystal waveguide[J]. Optics Express, 2016, 24(18): 20542-20553.
- [14] Sumi R, Das Gupta N, Das B K. Integrated optical linear edge filters using apodized sub-wavelength grating waveguides in SOI [J]. IEEE Photonics Technology Letters, 2019, 31(17): 1449-1452.
- [15] Charron D, St-Yves J, Jafari O, et al. Subwavelength-grating contradirectional couplers for large stopband filters[J]. Optics Letters, 2018, 43(4): 895-898.
- [16] Boroojerdi M T, Ménard M, Kirk A G. Wavelength tunable integrated add-drop filter with 10.6 nm bandwidth adjustability [J]. Optics Express, 2016, 24(19): 22043-22050.
- [17] Yun H, Hammond M, Lin S, et al. Broadband flat-top SOI add-drop filters using apodized sub-wavelength grating contradirectional couplers[J]. Optics Letters, 2019, 44(20): 4929-4932.
- [18] Hammond M, Mistry A, Yun H, et al. Broadband, silicon photonic, optical add-drop filters with 3 dB bandwidths up to 11 THz[J]. Optics Letters, 2021, 46(11): 2738-2741.
- [19] 廖莎莎, 包航, 冯玉婷, 等. 基于级联啁啾亚波长光栅辅助双向耦合器的超宽带可调滤波器[J]. 光学学报, 2022, 42(14): 1405003.
- [20] Liao S S, Bao H, Feng Y T, et al. Ultra-broadband tunable filter based on cascaded chirped subwavelength grating assisted contra-directional coupler[J]. Acta Optica Sinica, 2022, 42(14): 1405003.
- [21] 廖莎莎, 黄琼, 冯玉婷, 等. 高Q值、超窄带宽双向耦合型相移光栅[J]. 光学学报, 2023, 43(1): 0105001.
- [22] Liao S S, Huang C, Feng Y T, et al. Contra-directional coupling phase-shifted grating with high Q-factor and ultra-narrow bandwidth[J]. Acta Optica Sinica, 2023, 43(1): 0105001.
- [23] Ogusu K. Simple apodization technique for surface-corrugated waveguide gratings[J]. Optics Communications, 2018, 427: 180-183.

Ultra-High-Bandwidth Silicon-Based Photonic Filter for Coarse Wavelength Division Multiplexing Systems

Liao Shasha^{1,2*}, Huang Cong¹, Feng Yuting¹, Zhang Wuhan¹, Zhao Shuai¹, Liu Zhenwei¹

¹School of Communication and Information Engineering, Chongqing University of Posts and Telecommunications, Chongqing 400065, China;

²State Key Laboratory of Advanced Optical Communication Systems and Networks, Shanghai Jiao Tong University, Shanghai 200240, China

Abstract

Objective With the continuous development of scientific and technological information, people's demand for communication system capacity and speed is increasing, and wavelength division multiplexing technology plays an important role in improving system capacity. As a key component of wavelength division multiplexing systems, the demultiplexer has become a research hotspot in this field. At present, a large-bandwidth filter with a high rectangular degree is mainly used to realize the function of demultiplexing. High-bandwidth and ultra-high-bandwidth filter schemes are frequently proposed and implemented, involving photonic crystals, Mach-Zehnder interferometers, and waveguide Bragg gratings. Although traditional schemes based on photonic crystals and waveguide Bragg gratings can achieve large bandwidths, additional magneto-optical devices such as optical circulators need to be added to separate the reflected signals due to their working in the reflection mode, which undoubtedly increases the complexity of the system. In addition, the difficulty in the large-scale integration of magneto-optical materials with silicon-based devices also affects the application range of the above schemes. The Mach-Zehnder interferometer scheme is also difficult to integrate on a large scale due to its large structure size. Therefore, to realize a compact ultra-high-bandwidth filter, this paper proposes a filtering scheme based on a grating-assisted contra-directional coupler structure. The filter has the advantages of a high rectangular degree, an ultra-high bandwidth, and a low loss and can meet the needs of demultiplexing in coarse wavelength division multiplexing systems.

Methods To reduce the use of magneto-optical devices such as optical circulators and improve integration, this paper uses a grating-assisted contra-directional coupler structure to realize the filter function. According to the coupled mode theory, the bandwidth of the contra-directional coupler is inversely proportional to the sum of the effective refractive

indices of the two waveguides and proportional to the coupling coefficient. Therefore, it is necessary to reduce the effective refractive indices of the two waveguides and increase the coupling coefficient for enhancing the bandwidth of the filter. This paper first compares the effective refractive indices of sub-wavelength grating and conventional waveguide grating and finds that the former has a lower refractive index. Considering that a smaller waveguide width corresponds to a lower effective refractive index, the paper proposes to gradually change the input waveguide into a narrow waveguide through a taper so that the effective refractive index can be further reduced. When the width of the waveguide is reduced to a certain extent, the effective refractive index is lower than that of the current common scheme. Moreover, the narrow waveguide has a more dispersed electric field, which is beneficial to improve the coupling coefficient and achieve an ultra-high bandwidth. Therefore, in this paper, the narrow waveguide structure and the grating-assisted contra-directional coupler structure are used to address the low bandwidth, and the problem of a large structure size is also solved by continuing to optimize parameters.

Results and Discussions The width of the proposed narrow waveguide is 180 nm; the widths of the conventional grating and the sub-wavelength grating are both 500 nm; the duty cycle is 0.5. The effective refractive index of the narrow waveguide in the wavelength range of 1530–1570 nm is 1.441–1.447, which is smaller than those of the conventional grating and the sub-wavelength grating (Fig. 2). To further verify that the filter can achieve higher bandwidth, the transmission matrix method is used to calculate its spectral characteristics. At this time, the 3 dB bandwidth at the drop end is 70 nm (Fig. 3), which is in line with the above theoretical derivation. The grating comb and the waveguide are apodized at the same time to further improve the side-lobe suppression ratio (Fig. 5). In such a case, the 3 dB bandwidth of the filter is 92.9 nm; the side-lobe suppression ratio is greater than 11.1 dB; the shape factor is 0.99; the insertion loss is less than 0.38 dB; the in-band ripple is less than 0.28 dB (Fig. 6). This paper also designs a filtering scheme with a more compact structure and a higher side-lobe suppression ratio. After re-optimization, the 3 dB bandwidth is 87 nm; the side-lobe suppression ratio is 25.6 dB; the device length is 96 μm ; the insertion loss is 0.16 dB; the in-band ripple is 0.08 dB (Fig. 7).

Conclusions This paper proposes an ultra-high-bandwidth filter based on a grating-assisted contra-directional coupler. Firstly, in light of the coupled mode theory, the expression of the filter bandwidth is deduced, and the factors influencing the bandwidth are analyzed. Secondly, the paper develops a method of changing one waveguide in the contra-directional coupler to a narrow waveguide. After design and optimization, an ultra-high-bandwidth silicon-based photonic filter is finally realized with a 3 dB bandwidth of 92.9 nm, a side-lobe suppression ratio of 11.1 dB, a shape factor of 0.99, an insertion loss of 0.38 dB, and an in-band ripple of 0.28 dB. In addition, this paper also designs a filtering scheme with a more compact structure and a higher side-lobe suppression ratio. After re-optimization, the 3 dB bandwidth is 87 nm; the side-lobe suppression ratio is 25.6 dB; the device length is 96 μm ; the insertion loss is 0.16 dB; the in-band ripple is 0.08 dB. The two filter schemes proposed in this paper adopt the contra-directional coupling method. The filter bandwidth in scheme 1 is larger than the largest bandwidth of similar structures, and the scheme greatly reduces the size of the filter. Scheme 2 improves the side-lobe suppression ratio and reduces the length of the device, which is suitable for application scenarios that are more sensitive to side-lobe suppression ratio and size. In addition, this paper also focuses on analyzing the filter performance changes when there are process errors in the apodization coefficient and comb width of the grating. A method of increasing the design value of the gap G between the narrow waveguide and the grating and fine-tuning the grating period is proposed to reduce the influence of process errors on filter performance.

Key words integrated optics; coarse wavelength division multiplexing; silicon photonics; filter; photonic integrated circuits